Magnetoresponsive Devices with Programmable Behavior Using a Customized Commercial Stereolithographic 3D Printer

Magneto-responsive devices with programmable behavior using a customized commercial stereolithographic 3D printer

Simone Lantean [1,2], Ignazio Roppolo [1,3*], Marco Sangermano[1], Marc Hayoun[2], Hichem Dammak [2,4], Gabriele Barrera[5], Paola Tiberto[5], Candido Fabrizio Pirri[1,3], Laurence Bodelot[6], Giancarlo Rizza[2]

1. Department of Applied Science and Technology, Politecnico di Torino, Duca degli Abruzzi, 24, 10124, Torino, Italy
2. Laboratoire des Solides Irradiés (LSI), Institut Polytechnique de Paris, CEA/DRF/IRAMIS, CNRS, École polytechnique, Route de Saclay, 91128 Palaiseau, France
3. Center for Sustainable Future Technologies, Istituto Italiano di Tecnologia, Via Livorno 60, 10144, Torino, Italy
4. Laboratoire Structures Propriétés et Modélisation des Solides, CentraleSupélec, CNRS, Université Paris-Saclay, F 91190 Gif-sur-Yvette, France
5. Advanced Materials for Metrology and Life Sciences Division INRiM Strada delle Cacce 91, 10143 Torino, Italy
6. Laboratoire de Mécanique des Solides (LMS), CNRS, École polytechnique, Institut Polytechnique de Paris, Route de Saclay, 91128 Palaiseau, France

E-mail: ignazio.roppolo@polito.it

Keywords: 4D printing, magnetic device, programmed microstructure, magnetic actuation

Abstract

The revolution of 4D printing allows combining smart materials to additive processes to create behavioral objects able to respond to external stimuli, such as temperature, light, electrical or magnetic fields. Here, we use a modified commercial Digital Light Processing (DLP) 3D printer to obtain complex macroscopic remotely-controlled gear-based devices. The fabrication process is based on the printing of magneto-responsive polymers containing *in situ* self-assembled microstructures, i.e., composed of oriented chains of Fe_3O_4 nanoparticles. First, we demonstrate that we are able to print magneto-responsive hammer-like actuators with different stiffness allowing both pure rotation or/and bending motions. Then, we exploit the microstructure to create a magneto-responsive gear. In particular, we show that they can be successfully used to transfer torque to other gears, thereby converting a rotation movement into linear translation. Finally, we demonstrate that magneto-responsive gears can also be combined with other non-magnetic elements to create complex assemblies, such as gear-trains, linear actuators and grippers, that can be remotely controlled.

1. Introduction

Materials science is continuously inspired by Nature. Millions of years of evolution led living matter to develop an endless number of architectures and peculiar properties, as the ability to undergo motion in response to environmental stimuli [1,2]. For instance, in abalone shells and shrimps the oriented and hierarchical microstructure is responsible for their outstanding impact resistance [3,4], in carnivorous plants, as the Dionaea muscipula, the micro-structure is exploited to induce precise shape morphism, in pinecones the motion is actuated in response to humidity [5–9]. Magnetotactic bacteria synthesize magnetic iron nanominerals inside them, which function as tiny compasses allowing them to navigate by means of Earth's geomagnetic field. [10] From a technical point of view, despite the attempts to mimic and reproduce natural architectures and patterns, conventional fabrication techniques often face technical and resolution limitations. In the last years, this gap is being partially bridged thanks to the development of the 3D printing, where starting from a Computer-Aided Design (CAD) file, the final object is built through the additive deposition of material sub-units. However, the real breakthrough in this field of research has been to first imagine and then print behavioral objects [11]. This is the domain of the so-called 4D printing, which is, in a way, the functional form of 3D printing [12–14]. Instead of printing only static objects, it becomes possible to print functions. This paradigm shift allows a printed object to adapt to its environment and to evolve in a controlled way through the application of stimuli. So far, the 4D printing approach has been applied to functional polymers or composite materials such as hydrogels [15–18], electroactive polymers [19–21], shape memory polymers [22–26], or polymers sensitive to pH [27,28] and light [29,30]. Yet, the research on 4D printed objects with controlled microstructure is still in its infancy and it mainly focuses on the fabrication of composite materials with enhanced mechanical properties [31–40], where only a few works mentions the possibility to control the microstructure *in situ* during the printing process [41–46]. In particular, we are interested here in the tailor-made printing of magneto-reactive composite polymers [47–49]. Indeed, they can be easily actuated by remote magnetic fields without damaging tissues and organs, and thus be used for instance in soft robotics for healthcare and biomedical applications [50,51]. A first strategy to print magneto-responsive composite polymers consists in using hard magnetic fillers, such as $Nd_2Fe_{14}B$ micro-particles, and to orient their permanent dipoles using external strong magnets [52–54]. This process has been mainly applied in Fused Filament Fabrication (FFF) and Direct Ink Writing (DIW) 3D printing techniques [53,55]. In those cases, despite the fabrication of large objects in the X-Y plane, layer-to-layer adhesion issues generally limit their thickness to a few hundred microns

[55]. Furthermore, the use of such microparticles can be problematic in light-activated 3D printing (stereolithography and DLP) due to an increase in viscosity and to light scattering, which can affect the printing procedure.[56] A second strategy exploits the self-assembly of soft magnetic fillers, such as Fe_3O_4 nanoparticles (NPs) [57–59]. Magnetite is a low cost and earth-abundant material, available commercially in many forms, including NPs. When soft magnetic fillers are dispersed within a liquid medium and exposed to an external field, they spontaneously assemble into chain-like filamentary structures aligned along the field vector. The dimension and direction of the assembled chains, i.e., the microstructure, can be programmed by varying the experimental parameters such as the intensity of the applied magnetic field, the NPs concentration, and the viscosity of the medium [60–62]. The microstructure can be rapidly frozen by curing the formulation, embedding it in a matrix [60–62]. This creates a uniaxial magnetic anisotropy characterized by a magnetic easy axis (i.e., the major axis of the chains) along which the magnetic moments of single NPs are preferentially oriented, thereby forming an extended magnetic dipole in the chain [61–63]. This is particularly advantageous in light-activated technologies, and it can be exploited to actuate the printed object. Indeed, if an angle exists between the applied external magnetic field and the magnetic easy axis of the chains, a torque is exerted, which forces the object to rotate to align itself along the field vector [63–65]. Therefore, controlling the orientation of the magnetic microstructure allows programming the rotation and bending movements of the printed objects. So far, this approach has been mainly employed in 2D fabrication processes [66–69], in particular using a photo-lithographic approach, with the fabrication of multi-modal micro actuators [70]. More recently, the self-assembly process has also been applied to control the microstructure of twist-type micro-swimmers fabricated by Direct Laser Writing and actuated by external rotating fields [71–75], or to fabricate cellularized magneto-responsive hybrid hydrogels using a 3D bio-printing technique [76].

The present work is based on the knowledge we developed so far in the formulation of photocurable magneto-active acrylic resins [77], as well as the *in situ* control of the self-assembly of magnetite (Fe_3O_4) NPs during the printing process [78]. Here, our erstwhile knowledge is exploited to create macroscopic complex assemblies of magneto-driven elements, that can be remotely controlled. This is done in three steps: first, the formation of a controlled microstructure through the self-assembly of Fe_3O_4 NPs dispersed in photocurable resin as well as its spatial orientation have been investigated and rationalized by using numerical simulations. Second, we modified a commercial DLP printer [78] to obtain complex magneto-responsive objects, whose magnetic and mechanical properties have been measured for different formulations of the resin, different overall contents of magnetic fillers and different spatial

orientations of the microstructure. Finally, as a proof-of-concept, we fabricated different magneto-responsive devices: hammer-like actuators with different stiffnesses, as well as magneto-responsive gears. Additionally, we combined magneto-responsive components with non-magnetic elements to create complex assemblies, such as gear-trains, linear actuators and grippers, that can be remotely controlled.

2 Result and Discussion

The optimum condition to print magneto-responsive composite materials depends on three parameters: i) the average length of the self-assembled chains, ii) their spatial orientation, and iii) the concentration of the loaded magnetic fillers [78]. Fig. S1 illustrates the time evolution of the average length of self-assembled chains when exposed to a magnetic field of 10 mT. Here, the timeframe is limited to 180 s to be compatible with the printing process, and each point represents the average of at least 200 measurements. For both formulations, the chains' length reaches a plateau within 180 s; however, their values are quite different. Indeed, the formulation having the lower viscosity (50Eb50BA and open circles) leads to the formation of chains that are more than twice as long, i.e., ~50 μm, than those formed in the more viscous formulation (75Eb25BA and full circles), i.e., ~20 μm.

Once the chains of magnetic fillers have reached their saturation length, the microstructure can be spatially oriented by rotating the magnetic field. In this case, the aggregates will be submitted to a torque that will force the chains to re-orient their magnetic dipoles along the direction of the applied field [62,79–83], see Fig. S1, for the 50Eb50BA formulation. First, the self-assembly is triggered along θ_B=0, i.e., the horizontal direction, Fig. S1d. Then, to mimic the spatial orientation of the microstructure during the printing process, the magnetic field is rotated by $\theta_B = 30°$, Fig. S1e. In both cases, the numerical simulations correctly describe the dynamic evolution of the chains. After preliminary investigations on microscope slides, the formulations were tested for additive process on the modified DLP 3D printer. The necessary condition for obtaining objects with uniform magnetic properties is that the distribution of magnetic fillers inside the resin vat remains homogeneous throughout the printing process. Thus, the applied magnetic field has been first mapped by measuring its value in 13 different zones of the printing area as shown in Fig. 1b. Then, the stability of the NPs distribution was tested for at least 30 min, a time compatible with the duration of the fabrication of a 5 mm thick object. Configurations composed of A-A and AA-AA magnets produce quasi-homogeneous magnetic field distributions with an intensity at the center of the printing area of 5 mT and 10 mT,

respectively, and a gradient of about $\delta Gx \approx 1 \div 2$ mT.cm^{-1} (Figs. 1c,d). In both cases, a homogeneous distribution of the NPs within the printing area is observed as shown in Fig. 1e. In contrast, for the B-B, BB-BB and BA-AB configurations (Figs 1f-h)—producing a magnetic field at the center of the printing area of 11 mT, 20 mT and 15 mT, respectively, and a field gradient of about $\delta Gx \approx 5 \div 10$ mT.cm^{-1}—the migration of the fillers toward the edges of the ball bearing as well as the formation of a depleted central zone are observed, Fig. 1i. As the depletion process is driven by the gradient of the magnetic field [84], a value of $\delta Gx \approx 1 \div 2$ mT.cm^{-1} has been chosen as the upper threshold guaranteeing the homogeneous spatial distribution of the fillers during the printing step. In particular, the AA-AA configuration gives the optimum conditions to print magneto-responsive elements containing homogeneously distributed spatially oriented microstructures.

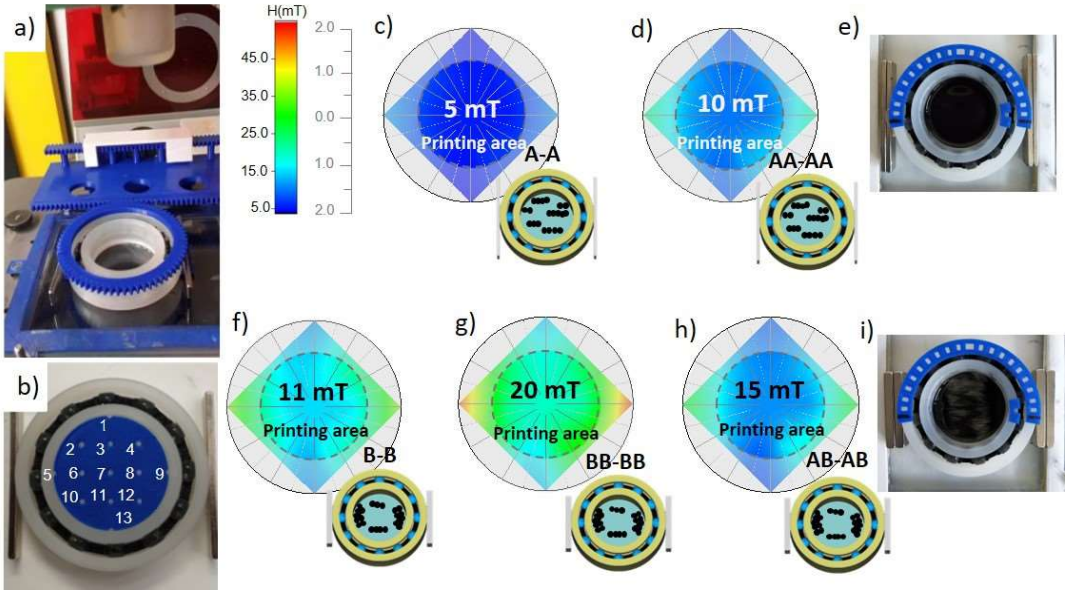

Figure 1. a) Modified DLP printer. b) Experimental mapping of the magnetic field distribution within the vat for several combinations of permanent magnets, named as A and B. A magnets are 60x10x2 mm^3 parallelepipeds exhibiting a magnetic field at the surface of 120 mT, while B magnets are 40x10x4 mm^3 parallelepipeds exhibiting a magnetic field at the surface of 310 mT. c) A-A and d) AA-AA configurations present e) a homogeneous distribution of the magnetic fillers dispersed within the photocurable resin. In contrast, for f) B-B, g) BB-BB and h) BA-AB configurations, i) inhomogeneities as well as depleted areas are observed in the vat.

The next step was the optimization of the processing parameters for the used formulations reported in Table 1. As expected, the curing time (i.e., the time necessary to cure a single layer) increases with the NPs concentration, while it is only slightly influenced by the concentration

of Butyl Acrylate (BA) [77]. On the other hand, the printing parameters are not modified by the applied magnetic field used to create the microstructure.

Field Emission Scanning Electron Microscopy (FESEM) was used to verify both the efficiency of the self-assembly process during the 3D printing phase and the incorporation of the magnetic chains within the polymer matrix. Figs. 2a1-c1 show that chains of magnetic fillers are systematically observed in each prepared sample. In addition, not only their length but also their width increases with the volume fraction of the embedded NPs with a subsequent effect on the aspect ratio of the chains. These results are confirmed by the numerical simulations (Figs. 2a2-c2) and can be easily understood by considering that the inter-particle distance decreases with increasing their load [85]. Thus, NPs are more likely to interact and yield larger assembled structures in highly-loaded systems than in dilute ones.

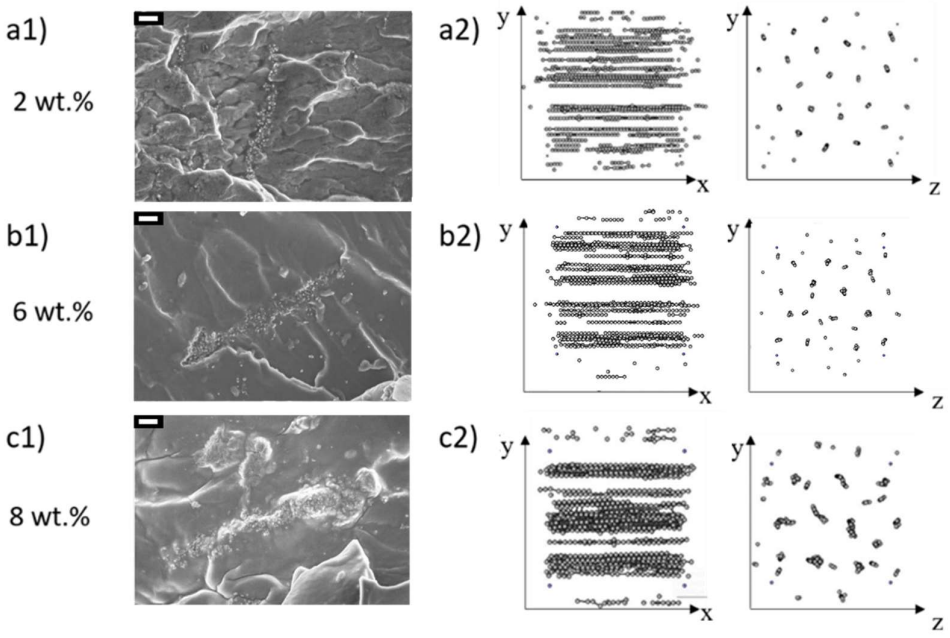

Figure 2. FESEM cross-section images of 3D printed 75Eb25BA samples with increasing content of magnetic fillers: a1) 2 wt.%, b1) 6 wt.%, c1) 8 wt.%. The scale bar is 20 µm. a2-c2) Numerical simulations based on a dipolar approximation model.

Finally, the printability of complex objects as well as the fidelity to the original CAD file have been validated for the 75Eb25BA and 50Eb50BA formulations containing 6 wt.% of magnetic fillers, by printing an Archimede's screw containing a microstructure spatially oriented by rotating the applied magnetic field (10 mT) by θ_B=30° every 20 printed layers, i.e., 400 µm of the printed object (Fig. 3). In Fig. 3, the original STL file (Fig. 3a) and the printed object (Fig. 3b) are shown together with a heat map (Fig. 3c) reporting the differences between the digital

file and the digitalization of the real object created by 3D scanning. As can be observed, the fidelity is very good (standard deviation 0.022 μm, average error about 100 μm).

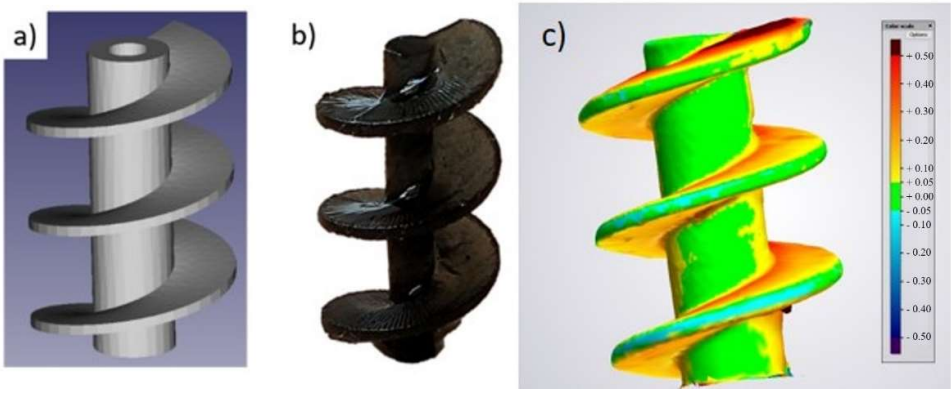

Figure 3. a) CAD file of an Archimede's screw used to check the feasibility and the fidelity of the printing process. b) Image of the printed object containing a spatially oriented microstructure. c) Heat map reporting the differences between the original stl file and the digitalization of the 3D printed object obtained by 3D scanning.

The magnetic properties of a 3D printed object containing an oriented microstructure were investigated on a 3x3x3 mm cubic specimen, as reported in Fig. 4a. The magnetic behavior of the sample containing 6 wt.% of Fe_3O_4 NPs (shown in Fig. 4 b-e) is representative of all the synthetized composites loaded with different NPs concentrations. Fig. 4b shows the sample containing a random dispersion of magnetic fillers. It is characterized by a perfect overlap of the hysteresis loops measured along the x, y and z axes, which in turn results in an isotropic magnetic behavior along these three equivalent directions of symmetry. In particular, the magnetization curves display the same hysteretic and reversal behavior with coercive field ($\mu_0 H_c$) of ≈ 12.8 mT and normalized remanent magnetization ($M_r/M_{1.5T}$) of ≈ 0.12. Conversely, the presence of chain-like structures makes the magnetic response of the printed cube anisotropic, i.e., the magnetic properties depend on the relative direction of the applied magnetic field with respect to the major axis of the chains, see Figs 4c-e. In particular, when the magnetic field is applied along the major axis of the chains (i.e., the magnetic easy axis)—black curve in Fig 4c for the chains aligned along the x-direction and red curve in Fig 4d for the chains aligned along the y-direction—the hysteresis loops appear steeper with a faster approach to saturation than those obtained with the magnetic field applied in the other directions (i.e., magnetic hard axes). Instead, for the sample where the chains are at 45°, Fig. 4e, the hysteresis loops measured along the x and y directions are now superimposed since, in this case, they are equivalent directions of symmetry with respect to the major axis of the chains. Of

course, the magnetic response measured along these two equivalent directions is intermediate with respect to the ones measured along the magnetic easy and hard axes. The z-direction corresponds to the only magnetic hard axis, as confirmed by the slower approach to magnetic saturation. In all samples, as expected, a reduction of the H_c and $M_r/M_{1.5T}$ values occurs from the easy axis to the hard one, insets in Figs 4c-e.

Cylindrical specimens with randomly distributed or oriented NPs were produced with the modified DLP 3D printer (example in Fig. 4f). The polar plot of $M_\perp$ measured for both randomly distributed (black curve) and self-assembled NPs (red curve) is reported in Fig. 4g, showing the symmetry of the magnetic anisotropy induced by the microstructure of the magnetic filler. The approximately round shape of the black curve indicates an almost perfectly isotropic magnetic behavior for the sample containing randomly distributed NPs. Conversely, a two-lobe profile is observed in the sample containing magnetic chains (red curve), which is the fingerprint of the presence of a uniaxial anisotropy within the sample,[86] i.e., only one easy axis of magnetization originates from the elongated shape of the magnetic chains.

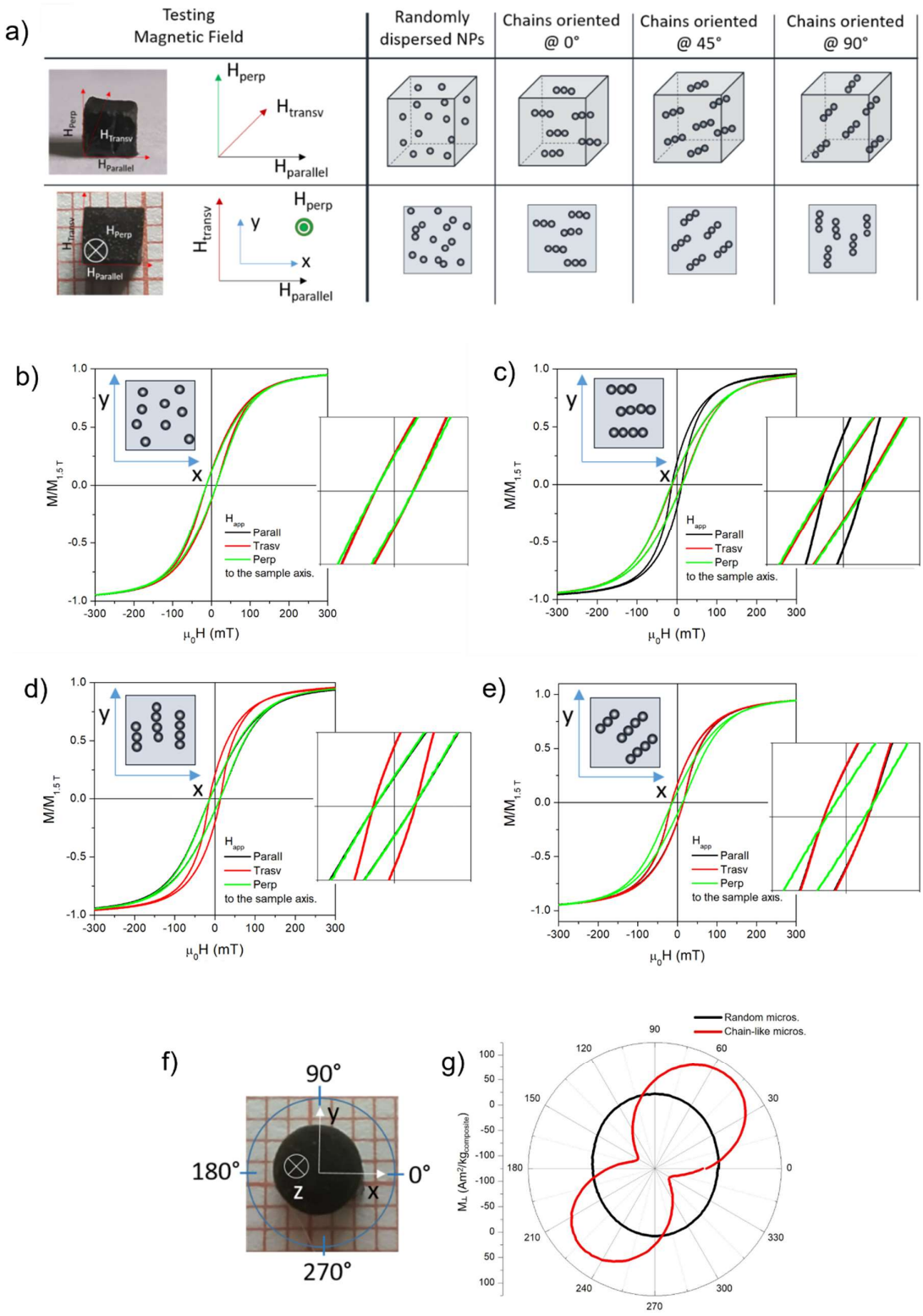

Figure 4. a) Sketch of configuration used to measure the magnetic response of a 3D printed cube. Two configurations have been probed: randomly dispersed NPs, and chains of NPs aligned along x-direction (0°), y-direction (90°) and at 45°. Magnetic hysteresis loops measured along the x (black line), y (red line) and z (green line) directions for the 75Eb25BA_6NPs samples differing by their microstructure: b) randomly dispersed NPs, c)

chains oriented at 0°, d) chains oriented at 90°, e) chains oriented at 45° with respect to the x-direction. f) 3D printed cylinder used to measure the angular dependence of the magnetic anisotropy. g) Polar plots for the perpendicular (M⊥) component of the magnetization; black curve: Fe_3O_4 nanoparticles homogenously distributed; red curve: Fe_3O_4 nanoparticles self-assembled into a chain structure. Direction is approximately 50°.

Using the magnetic susceptibility at the coercive field (χ_c) as a probing parameter, it is possible determine the amount of magnetic fillers in the printed objects that maximizes the anisotropic magnetic response. The χ_c values measured both parallel (full squares) and perpendicular (open circles) to the chains' major axis from the corresponding hysteresis loops are shown in Fig. S2. The value of χ_c corresponding to the randomly distributed NPs (gray dashed line) is used as reference. As expected, for all the concentrations of NPs up to 8 wt.%, the parallel-χ_c values are systematically higher than the corresponding perpendicular-χ_c values indicating a magnetic anisotropic effect. However, the parallel-χ_c shows a non-monotonic behavior, where an increase as a function of the concentration of magnetic NPs is observed up to 4 wt.% at which a value of about 20 T^{-1} is reached. This value remains almost constant up to 6 wt.%, and then decreases at 8 wt.% to a value close to the one obtained for samples loaded with 0.5 wt.% of NPs. On the other hand, the perpendicular-χ_c values remain almost constant at about 8.5 T^{-1} close to the reference value (gray dashed line) regardless of the concentration of fillers. Thus, two conclusions can be drawn: i) the magnitude of magnetic susceptibility in the direction of the magnetic anisotropy can be tuned by the amount of NPs loaded in the polymer, with an optimum concentration of the fillers in the range 4-6 wt.%; ii) along the direction perpendicular to the chains' major axis, the effect of the anisotropy is weak. Moreover, the magnitude of the magnetic susceptibility in the directions perpendicular to the easy axis is almost independent on the NPs concentration as it is observed that the magnetization reversal mechanism is very similar to that of uniformly dispersed NPs.

An estimate of the average chains' aspect ratio (α) and of the contribution to the effective magnetic anisotropy by the chain shape (K_s) has been obtained by using the procedure described in the SI and is reported in Fig. S3c for all Fe_3O_4-loaded printed samples. The value of α shows a non-monotonic behavior with a maximum value of about 1.8 for a NP concentration in the range 4-6 wt.%. This suggests that an initial increase in NP concentration within the polymer composite leads to the formation of longer chains, in agreement with SEM observations and numerical simulations (see Fig. 2) as well as existing literature [62,87,88]. On the other hand, the reduced value of α observed for a load of 8 wt.% can be explained by the fact that when the amount of embedded NPs overcomes a threshold value, the self-assembly process forms overlapping and interconnected magnetic chains (see Fig.2c2). Therefore, the chains no longer

act as isolated magnetic units but as larger and interacting magnetic assemblies. This affects the overall magnetic behavior by reducing the contribution to the effective magnetic anisotropy, and in turn by decreasing the magnetic susceptibility of the composite material. In addition, the evolution of K_s values, also shown in Fig. S3c, has a similar trend to that of α with a maximum value of about $6.3x10^3$ J/m^3 in the range 4-6 wt.% of embedded NPs, which thus represents the optimum load of magnetic fillers. These results show the effectiveness of the magnetic field-driven self-assembly process during the DLP printing step to program the effective magnetic anisotropy of the polymer composite, which in turn induces a net magnetic moment capable of yielding an actuation motion by magnetic torque.

We previously demonstrated that the mechanical properties (e.g., stiffness) of the printed composite can be tuned by varying the amount of BA in the Ebecryl (Eb) resin, and that the optimum concentration of fillers for the printing process under the application of a constant magnetic field of 10 mT is 6 wt.% [77, 78]. Here, the effect of the orientation of the chains on the mechanical properties of the printed materials was studied (Fig. S4). For the stiffer sample (75Eb25BA_6NPs), the value of the elastic modulus is, within the error bar, equivalent to that of the reference sample, i.e., E~4.5 MPa. Thus, the orientation of the microstructure does not alter the mechanical response of the composites when subjected to tensile stress. For the softer sample (50Eb50BA_6NPs), a reduction of the elastic modulus of about 10 % is observed with respect to the reference sample containing only dispersed NPs, i.e., E~3.75 MPa. This is presumably due to the incorporation of larger aggregate-inducing defects, as already observed in soft samples [77].

Once both the magnetic and mechanical properties of the 3D printed materials with oriented nanoparticles were studied in detail, the information was subsequently employed to develop 3D printed objects with programmed response, and finally 3D printed magnetic devices, exploiting magnetic fields. Indeed, when a 3D printed device containing a magnetic microstructure is subjected to an external magnetic field, a magnetic torque (τ_m) is exerted on the extended magnetic dipole, which forces the chains to rotate in order to align their easy magnetic axis along the field direction [65,70,89–93]. In general, the magnetic torque can be expressed as: $\tau_m = dU_m/d\theta$, where U_m is the magnetic energy of the material and θ is the rotation angle. Approximating a chain to a prolate ellipsoid with a and b its long and short dimensions, U_m can be written as [65]:

$$U_m = \frac{2\pi ab^2}{3}\frac{\bar{\chi}^2}{\bar{\chi}+2}\mu_0 H^2 \sin^2\theta \quad (1)$$

where $\bar{\chi} = 3\chi/\chi + 2$ is the shape-corrected susceptibility of the magnetic unit and H is the applied magnetic field. When the magnetic chains are confined within and anchored to the host polymeric matrix, the torque is transferred to the whole material. In this case, two pathways are possible: if the composite is rigid it will be subject to an overall rotation; conversely, if the composite is soft and the magnetic torque overcomes the mechanical resistance of the material, the object will deform [65,70,93]. Thus, using the modified DLP printer to control the microstructure during the printing process, as well as the initial formulation to tune the stiffness of the printed sample, several magnetically-driven actuators have been obtained.

First, rigid hammer-like structures undergoing predefined rotations were obtained. The magneto-responsive hammers were 3D printed using the 75Eb25BA formulation loaded with 6 wt.% of NPs, 75Eb25BA_6NPs (Fig. 5a). Five hammers were printed, each having a defined orientation of the microstructure, i.e., 0°, 45°, 90°, 135°, and 180° as indicated by the arrows in Fig. 5b. To minimize the friction effects, the hammers were placed in a petri dish filled with water and each hammer was anchored to a pinion of a 3D printed rack. Their rotations were studied by using a pair of Helmholtz coils generating a magnetic field up to 4 mT in the x-y plane, Fig. S5 in SI.

In the initial configuration, the magnetic field is switched off (H=0) and all the hammers are parallel one to another as shown in Fig. 5c. As soon as the field is applied (H=+4 mT) in the direction indicated in Fig. 5d, each hammer starts to rotate around its anchoring point until the equilibrium configuration is reached, Fig. 5e. This is until the microstructure, indicated by the arrow, aligns with the direction of the applied field. As each hammer has a specific microstructure, they rotate at a different angle. By reversing the direction of the applied field (H=-4 mT), it is possible to reverse the process, Fig. 5f. Finally, the repeatability of the process is demonstrated by inverting again the direction of the applied field (H=+4 mT), Figs. 5g-h. A complete sequence of the controlled motion of these actuators is reported in video S1.

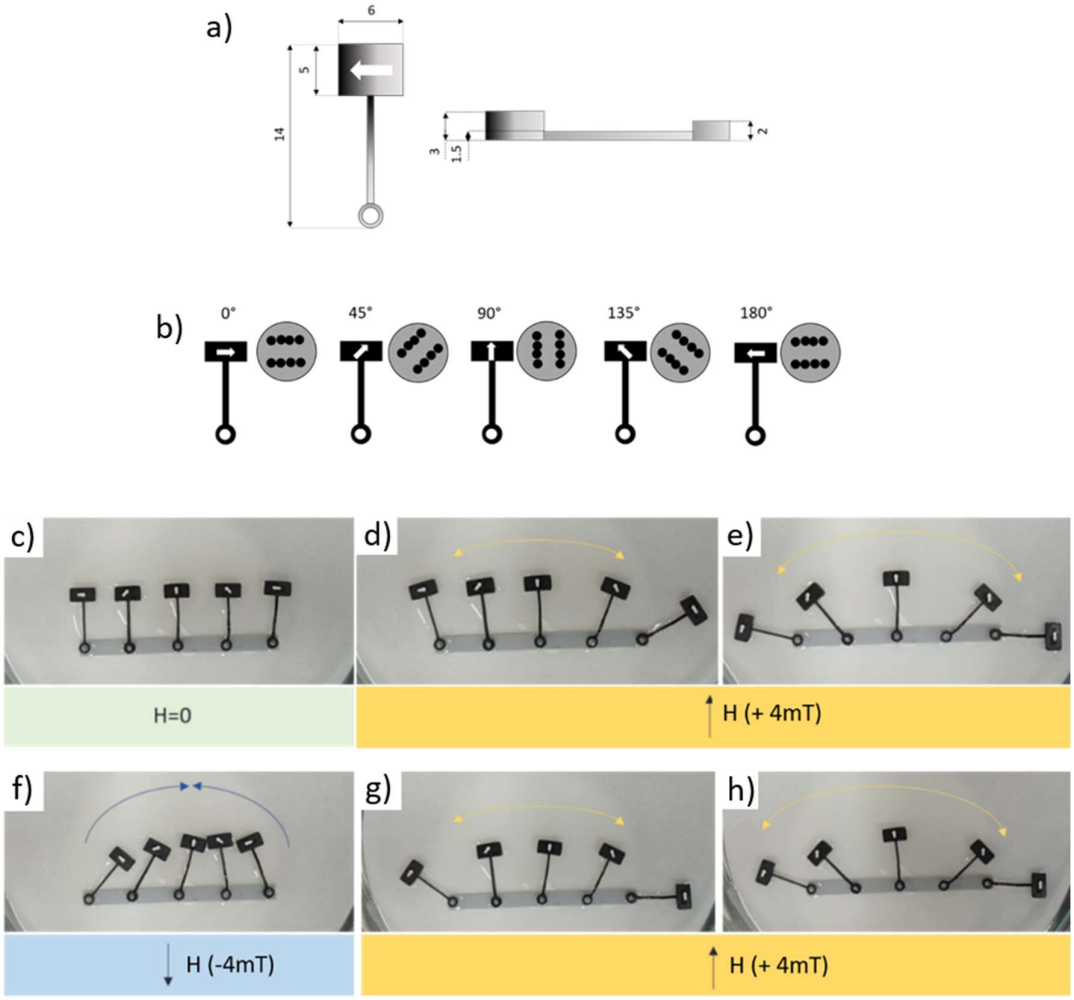

Figure 5. a) Dimensions of the 3D printed rigid magnetic hammers (mm) and b) orientation of the microstructure within each hammer. c-h) Time evolution of rigid magneto-responsive hammers having different orientations of the microstructure (indicated by the arrows) as a function of the applied magnetic field.

A similar approach was then used to exploit the bending of printed soft composites. In this case, the magnetic force ($\tau_{Magnetic}$) must overcome the mechanical resistance of the material ($\tau_{Mechanic}$) to obtain bending. Thus, magneto-responsive flexible actuators can be printed by either increasing the intensity of the applied magnetic field or by reducing the mechanical resistance of the sample. The latter option can be obtained either by tuning the stiffness of the matrix and/or by changing the geometry of the sample. In the present case, both the mechanical properties of the object and its design have been adapted. In particular, a soft hammer was printed using the 50Eb50BA formulation loaded with 6 wt.% of NPs (50Eb50BA_6NPs) and its mechanical resistance was decreased by locally reducing the thickness of the hammer's arm as indicated in Fig. 6a. Again, friction effects have been minimized by placing the hammer in

a petri dish filled with water. Contrarily to the rigid hammers, the extremity of the flexible hammer was fixed to a support for preventing the object to rotate. As the bending of a millimeter-size actuator necessitates an intensity of the magnetic field larger than the one that can be obtained using standard Helmholtz coils, a couple of NdFeB permanent magnets have been used to activate the actuation process as described in SI. The initial configuration (H=0) is shown in Fig. 6b, where the orientation of the microstructure is indicated by the arrow. A magnetic field is then applied normally to the microstructure, whose magnitude was tuned by an Arduino controller by varying the relative distance between a couple of magnets. Below a critical distance the magnetic torque (τ_{mag}) overcomes the mechanical one (τ_{mech}) and the hammer starts bending to re-align its easy magnetic axis in the direction of the field, Fig. 6c. As expected, when reversing the polarity of the magnets, the bending is observed in the opposite direction, Fig. 6d. The complete sequence of the bending of the hammer is reported in video S2.

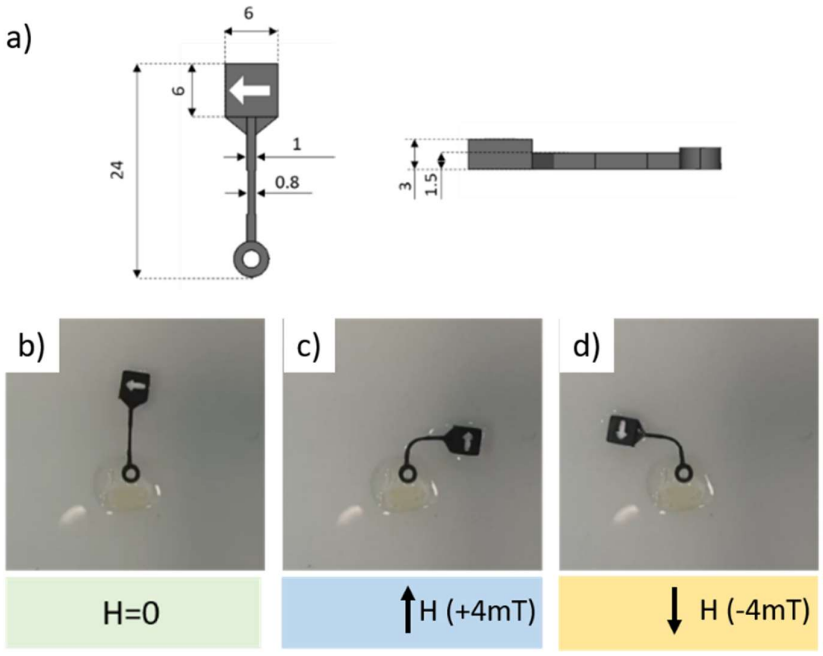

Figure 6: a) Design of a magneto-responsive soft hammer. The microstructure is indicated by the arrow on the head of the hammer. b) Initial configuration (H=0) and c)-d) bending of the magneto-responsive soft hammer for two opposite directions of the applied magnetic field.

To increase the degree of complexity on our objects we checked the possibility to 3D print magnetically-driven gears. Mechanical gears are toothed wheels that transmit rotation and power from one shaft to another, or that work in combination with one or more other gears to

alter the relationship between the speeds of the driver and the driven parts. Magnetic gears, first patented by Armstrong in 1901 [94], resemble the traditional mechanical gears in geometry and function, except that the force/torque transmission exerted by tooth meshing is replaced with the contactless magnetic interaction. As two opposing magnets approach each other, they repel; when placed on two rings the magnets will act like teeth.

First, the feasibility of remote control of gear rotation has been verified by printing two identical elements, i.e., using the same formulation (75Eb25BA_6NPs) and the same design (10 teeth, 1 mm module, and a pressure angle of 20°), but with different microstructures (oriented and dispersed NPs) as reported in Fig. S6. The reversibility of the process has been checked by switching the magnetic field several times. The complete sequence is reported in Fig. S6 and in video S3. The interpretation of these experimental results is quite straightforward, and it is clearly related to the different microstructures of the two objects. On one hand, a sample containing dispersed NPs is magnetically isotropic as indicated by the hysteresis cycles (Fig. 4b), thus the application of a uniform magnetic field does not generate a net magnetic torque, and the rotation of the sample is nearly absent. On the other hand, the presence of a microstructure in the sample creates a magnetic anisotropy in the object, which in turn generates a magnetic torque ($\sim M_{easy} \times H$) forcing the gear to rotate.

When two or more gears are linked together, the ensemble is considered as a gear train where the "input gear" (also known as drive gear) transmits the power to the "output gear" (also known as driven gear), Fig. S7. In a standard gear train, the input gear is typically connected to a power source, such as a DC motor. In this case, the magneto-active drive gear is remotely controlled by an external magnetic field, and the driven gear is non-magnetic and printed using an inert resin. The complete sequence of work is reported in the Supporting Information of this manuscript (Fig. S7 and video S4).

A further step was to fabricate a linear actuator composed of a spur gear and a linear rack coupled together through the meshing of their respective teeth. The complete sequence as well as the explanation of the process is reported in the Supporting Information of this manuscript (Fig. S8).

The linear actuator was then employed to build a magnetic driven gripper. Generally speaking, grasping is the ability to pick up and hold an object, while manipulation is the ability to produce rotation and displacement. Grasping and manipulation are two functions that are of paramount importance in robotics as they allow the machine to mimic the behavior of human beings and animals. This device is composed of two non-magnetic clamping arms activated by a magneto-responsive linear actuator. In the literature, some magnetically-driven grippers have been

reported, but they are based on the 3D printing of magnetic composites [95,96]. In contrast, in the present case, the magnetic component was decoupled from the gripping part, allowing remote control without the necessity to insert magnets close to the gripping part, but instead exploiting the programmed microstructure of the gears. The operation of this magneto-responsive gripper is illustrated in Fig. 7a-g. In the initial configuration, the two arms of the grippers are in the open position, i.e., they are far from each other. When the magnetic field is switched on, the magneto-responsive drive gear stars to rotate anti-clockwise, transferring its motion to the rack. Then, a couple of driven gears transform again the translating motion of the rack into a rotary one. As they have been printed with an arm and a clamp, they play the role of the hands of the gripper. Inverting the field allows the magneto-responsive spur gear to rotate clockwise, and the arms of the gripper to open up and return to their initial configuration. The complete sequence is reported in the Supporting Information of this manuscript (video S5). This proof-of-concept example indicates that the development of magneto-responsive devices with advanced functionalities is technically possible.

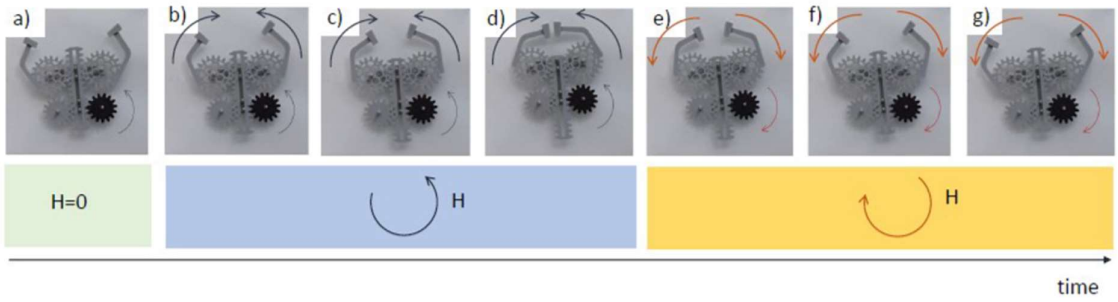

Figure 7: a-g) Timeframe evolution of the magnetically-driven clamp driven by a magneto-active drive gear.

3. Conclusion

Magneto-responsive polymers with oriented microstructures behave as magnetic compasses. Indeed, when a uniform magnetic field is applied, the composite sample undergo rotation movements (if rigid) or bending (if soft) to align its easy magnetic axis along the field lines. Taking advantage of this phenomenon, we printed magnetically-driven macroscopic elements undergoing programmed movements by the remote application of a magnetic field. Our approach is based on the ability to tune the self-assembly of the magnetic microstructure (Fe_3O_4) and to control its orientation in a photocurable resin during the printing process thanks to the modification of a DLP-type printer.

In this work, our approach is first applied to fabricate magneto-responsive hammer-like actuators with different stiffnesses allowing both pure rotation or/and bending motions. As an application, these elements could be used to create a magneto-responsive electric-switch. Then, by introducing the idea that the microstructure can be exploited to create a magneto-responsive gear, we showed that the latter can be successfully used to transfer torque to other gears, thereby converting a rotation movement into linear translation. Finally, we demonstrated that magneto-responsive gears can be also combined with other non-magnetic elements to create complex assemblies, such as gear-trains, linear actuators and grippers, that can be remotely controlled. We believe that our approach can be further developed to achieve even more complex component systems and could generate new opportunities in robotics-related applications.

4. Experimental

4.1 Formulation

The magneto-active formulation is obtained by adding magnetite nanoparticles (Fe_3O_4 NPs, 50-100 nm diameter) to a photocurable Urethane Acrylate resin (Ebecryl® 8232) with different amount of Butyl Acrylate (BA) and using Phenylbis(2,4,6-trimethylbenzoyl)phosphine oxide (Merck) as the photoinitiator (1 wt.% of the monomers), as reported by Lantean *et al.* [77]. As demonstrated in this work, this last ingredient is used both to adjust the viscosity of the formulation and to control the mechanical properties. In particular, three different weight concentrations of BA have been considered (0%, 25%, and 50%), leading to three different formulations, hereafter named as 100Eb, 75Eb25BA, and 50Eb50BA. Their corresponding viscosity has been measured to be η=5.6 Pa.s, η=1.8 Pa.s, and η=0.02 Pa.s. Spherical shape magnetite (Fe_3O_4) nanoparticles with a nominal diameter ranging between 50-100 nm (98% purity) were purchased from Merck and used as received. Nanoparticles were dispersed in the formulation by stirring followed by sonication, following previously reported procedures [77]. Viscosity and photo-reactivity of the formulations have been used to tune both the mechanical properties of the printed object as well as the dimensions of the embedded chain-like aggregates of Fe_3O_4 NPs, as already reported by Lantean *et al.* [78].

4.2 Self-assembly-driven magnetic microstructure

The average length of the self-assembled chains, their spatial orientation, and the concentration of the loaded magnetic fillers have been studied *in situ* using a Leica DFC295 optical microscope equipped with a 10x optics, and experimental results have been rationalized by using numerical simulations based on a dipolar approximation model [78,97,98]. The viscosity effect has been investigated for the 75Eb25BA and 50Eb50BA formulations by coating, with the help of a wire wound bar, a 200 μm thick film on the surface of a microscope slide. This thickness has been chosen to mimic 10 layers (20 μm each) of a printed sample.

The orientation step is triggered by applying a 10 mT magnetic field in the horizontal direction ($\theta_B = 0$), with an initial waiting time of 180 s, to let the chains reach stable dimension. Those parameters were based on a previous study of Lantean *et al.*[77]. Then, the magnetic field is rotated by $\theta_B = 30°$ and the image taken 120 s after the rotation step. Experimental results have been coupled to numerical simulations on a system composed of 1,000 NPs using periodic boundary conditions [78,79]. The size of the cubic box depends on the weight fraction of NPs. More details can be found in the Supporting Information File.

4.3 DLP printer modification and printing parameters

The control of the microstructure within the printed composite polymers is obtained by using a modified DLP machine (RobotFactory HD 2.0+) as described in a previous work [77]. As shown in Fig. 1a-b, a linear-to-rotary actuator driven by an Arduino microcontroller is used to control the rotation of a non-magnetic ball-bearing glued on the bottom glass plate of the vat. Its role is twofold: i) the central hole acts as a resin reservoir, while ii) the rotating external wall is used to apply the magnetic field in the X-Y plane (H) by fixing to it two permanent magnets of suitable intensity. The intensity of the applied magnetic field has been tested by considering several combinations of permanent magnets, hereafter named as A and B (www.supermagnete.fr). The A magnet is a 60x10x2 mm^3 parallelepiped exhibiting a magnetic field at the surface of 120 mT, while the B magnet is a 40x10x5 mm^3 parallelepiped exhibiting a magnetic field at the surface of 310 mT. Finally, to fit with the new resin reservoir, the original building platform was modified by adding an appropriately sized glass cylinder.

The processing parameters have been determined for 75Eb25BA and 50Eb50BA formulations by printing rectangular samples (3 mm thick) for increasing concentration of Fe_3O_4 NPs (up to 8 wt.%) in the absence and presence of magnetic field, i.e., B=0 mT and B=10 mT, respectively. The thickness of each printed layer was set to be 20 μm. Table 1 reports the processing parameters for the different formulations. All the different structures tested along the

manuscript where 3D printed following these parameters. For the samples with oriented nanochains, before printing, a waiting time of 180 s was fixed to allow the formation of the chains in the printable formulations.

Table 1: Printing parameters used to 3D print the magneto composite polymers.

Sample	Alignment Magnetic field (mT)		Slicing (μm)	Base exposing time (s)	Object exposing time (s)
75Eb25BA_2wt.%NPs	0	10	20	2.9	1.6
75Eb25BA_4wt.%NPs	0	10	20	4.4	2
75Eb25BA_6wt.%NPs	0	10	20	5.8	2.4
75Eb25BA_8wt.%NPs	0	10	20	9.5	3
50Eb50BA_2wt.%NPs	0	10	20	2.9	1.4
50Eb50BA_4wt.%NPs	0	10	20	4.2	1.8
50Eb50BA_6wt.%NPs	0	10	20	5.5	2.2
50Eb50BA_8wt.%NPs	0	10	20	9.5	3

4.4 Characterization

The dispersion of magnetic fillers as well as their self-assembly in chains was investigated by using a Zeiss Supra 40 Field Emission Scanning Electron Microscopy (FESEM). Cryo-fracturing of photocured samples was used to avoid plastic deformation and filamentary aggregates.

The magnetic properties of the 3D printed objects have been investigated at room temperature by an Alternating Gradient Field Magnetometer (AGFM) operating with an applied magnetic field in the range -1.5 T up to +1.5 T. The hysteresis loops (i.e., the magnetization *vs.* applied magnetic field curves, M(H)) have been measured along the three symmetry equivalent directions—hereafter named as parallel (x-direction), transverse (y-direction), and perpendicular (z-direction) of a 3D printed cubic sample (3x3x3 mm^3). All magnetic curves have been normalized to the magnetic moment value at H = 1.5 T.

The hysteresis curve allows to evaluate the magnetic susceptibility, χ, which is defined by $\chi = M/H$. It describes the way in which M varies within the material as a function of the applied field H. As χ is a tensor, it can be used to estimate the magnetic behavior of the sample along different spatial directions. Here, the magnetic susceptibility measured at the coercive field of the hysteresis curve $\chi_c(H_c)$ has been selected as a physical indicator to estimate the degree of magnetic anisotropy in the sample.

Two microstructural configurations of printed samples loaded with 6 wt.% of Fe_3O_4 NPs have been investigated: i) randomly distributed NPs, and ii) self-assembled chains. For the latter,

chains are created before the additive step by applying a magnetic field of 10 mT in the x-y plane along three different directions, 0°, 45°, or 90° with respect to the x-direction.

Vector-Vibrating Sample Magnetometer (V-VSM) was used to study the angular dependence of the magnetic anisotropy in both samples. In particular, the component of magnetization (M⊥) perpendicular to the direction of the applied magnetic field was measured as a function of the angle during the relative rotation of the sample. To this end, samples with both randomly and filamentary distributed NPs were 3D printed with a cylindrical shape to avoid any magnetic anisotropy effect.

Dynamic Mechanical Thermal Analysis (DMTA) in tensile configuration (Triton Technology TTDMA equipment) was used to measure mechanical properties. Elongation tests were run at room temperature in load control (1N/min). The dimensions of the tested specimens are 30x4x3 mm^3 (length x width x thickness) with chains oriented at 0°, 45°, and 90° relative to the length of the sample. For comparison, 3D printed samples with randomly dispersed NPs are used as reference.

3D scanning of the 3D printed object was performed with a E3 scanner (3shape). The comparison heat map was obtained by the Convince software (3shape).

Authors Contribution

S.L. conducted the investigations and helped in the preparation of the first draft of the paper. I.R. and G.R. designed the research and supervised the results and data analysis, preparing the first draft of the paper. M.S., L.B. and C.F.P. performed data analysis and discussion of the results. M.H. and H.D. performed simulations. G.B. and P.T. performed magnetic characterization and analysis. All the authors contributed in writing and revised the paper.

Acknowledgements

This work was supported by Compagnia di San Paolo trough the “Joint Project with Top Universities” grant. This work has benefited from the financial support of the LabEx LaSIPS (ANR-10-LABX-0032-LaSIPS) managed by the French National Research Agency under the "Investissements d'avenir" program (ANR-11-IDEX-0003-02). This work was also performed using HPC resources from École Polytechnique through the LLR-LSI project and from the “Mésocentre” computing center of CentraleSupélec and École Normale Supérieure Paris-Saclay supported by CNRS and Région Île-de-France (http://mesocentre.centralesupelec.fr/).

References

[1] P. Fratzl, R. Weinkamer, *Prog. Mater. Sci.* **2007**, *52*, 1263. DOI 10.1016/j.pmatsci.2007.06.001

[2] P. Fratzl, *J. R. Soc. Interface* **2007**, *4*, 637. DOI 10.1098/RSIF.2007.0218

[3] J. C. Weaver, G. W. Milliron, A. Miserez, K. Evans-Lutterodt, S. Herrera, I. Gallana, W. J. Mershon, B. Swanson, P. Zavattieri, E. DiMasi, D. Kisailus, *Science.* **2012**, *336(6086)*, 1275-1280 DOI 10.1126/science.1218764.

[4] L. K. Grunenfelder, N. Suksangpanya, C. Salinas, G. Milliron, N. Yaraghi, S. Herrera, K. Evans-Lutterodt, S. R. Nutt, P. Zavattieri, D. Kisailus, in *Acta Biomater.*, **2014**, *10(9)*, 3997-4008**.** DOI 10.1016/j.actbio.2014.03.022.

[5] A. M. C. Emons, B. M. Mulder, *Trends Plant Sci.* **2000**, *5(1)*, 35-40 DOI 10.1016/S1360-1385(99)01507-1.

[6] I. Burgert, P. Fratzl, *Integr. Comp. Biol.* **2009**, *49(1)*, 69-79, DOI 10.1093/icb/icp026.

[7] A. Fabricant, G. Z. Iwata, S. Scherzer, L. Bougas, K. Rolfs, A. Jodko-Władzińska, J. Voigt, R. Hedrich, D. Budker, *Sci. Rep.* **2021**, *11*, 1438, DOI 10.1038/s41598-021-81114-w.

[8] R. Sachse, A. Westermeier, M. Mylo, J. Nadasdi, M. Bischoff, T. Speck, S. Poppinga, *Proc. Natl. Acad. Sci. U. S. A.* **2020**, *117(27)*, 16035-16042, DOI 10.1073/pnas.2002707117.

[9] A. Le Duigou, M. Castro, *Ind. Crops Prod.* **2017**, *99*, 142-149, DOI 10.1016/j.indcrop.2017.02.004.

[10] A. Scheffel, M. Gruska, D. Faivre, A. Linaourodis J.M. Plitzko, D. Schüler *Nature* **2006**, *440,* 110–114, DOI 10.1038/nature04382

[11] S. Tibbits, *Archit. Des.*, **2014**, *84(1)*, 116-121, DOI https://doi.org/10.1002/ad.1710**.**

[12] Z. X. Khoo, J. E. M. Teoh, Y. Liu, C. K. Chua, S. Yang, J. An, K. F. Leong, W. Y. Yeong, *Virtual Phys. Prototyp.* **2015**, 103-122, DOI 10.1080/17452759.2015.1097054.

[13] A. Mitchell, U. Lafont, M. Hołyńska, C. Semprimoschnig, *Addit. Manuf.*, **2018**, *24*, 606-626, DOI 10.1016/j.addma.2018.10.038.

[14] D. G. Shin, T. H. Kim, D. E. Kim, *Int. J. Precis. Eng. Manuf. - Green Technol.* **2017**,*4(3)*, 349-357, DOI 10.1007/s40684-017-0040-z.

[15] S. E. Bakarich, R. Gorkin, M. In Het Panhuis, G. M. Spinks, *Macromol. Rapid Commun.* **2015**, *36(12)*, 1211-1217, DOI 10.1002/marc.201500079.

[16] Y. Hu, Z. Wang, D. Jin, C. Zhang, R. Sun, Z. Li, K. Hu, J. Ni, Z. Cai, D. Pan, X. Wang, W. Zhu, J. Li, D. Wu, L. Zhang, J. Chu, *Adv. Funct. Mater.* **2020**, *30(4)*,

1907377, DOI 10.1002/adfm.201907377.

[17] J. Guo, R. Zhang, L. Zhang, X. Cao, *ACS Macro Lett.* **2018**, *7(4)*, 442-446, DOI 10.1021/acsmacrolett.7b00957.

[18] M. N. I. Shiblee, K. Ahmed, M. Kawakami, H. Furukawa, *Adv. Mater. Technol.* **2019**, *4(8)*, 1900071, DOI 10.1002/admt.201900071.

[19] L. H. Shao, B. Zhao, Q. Zhang, Y. Xing, K. Zhang, *Extrem. Mech. Lett.* **2020**, *39*, 100793, DOI 10.1016/j.eml.2020.100793.

[20] D. Grinberg, S. Siddique, M. Q. Le, R. Liang, J. F. Capsal, P. J. Cottinet, *J. Polym. Sci. Part B Polym. Phys.* **2019**, 57(2), 109-115, DOI 10.1002/polb.24763.

[21] T. Mirfakhrai, J. D. W. Madden, R. H. Baughman, *Mater. Today* **2007**, *10(4)*, 30-38, DOI 10.1016/S1369-7021(07)70048-2.

[22] H. Meng, G. Li, *Polymer (Guildf).* **2013**, *54(9)*, 2199-2221, DOI 10.1016/j.polymer.2013.02.023.

[23] J. Wu, C. Yuan, Z. Ding, M. Isakov, Y. Mao, T. Wang, M. L. Dunn, H. J. Qi, *Sci. Rep.* **2016**, *6*, 24224, DOI 10.1038/srep24224.

[24] K. Yu, A. Ritchie, Y. Mao, M. L. Dunn, H. J. Qi, in *Procedia IUTAM*, **2015**. *12*, 193-293, DOI 10.1016/j.piutam.2014.12.021

[25] Y. Mao, K. Yu, M. S. Isakov, J. Wu, M. L. Dunn, H. Jerry Qi, *Sci. Rep.* **2015**, *5*, 13616, DOI 10.1038/srep13616.

[26] M. Zarek, M. Layani, I. Cooperstein, E. Sachyani, D. Cohn, S. Magdassi, *Adv. Mater.* **2016**, *28(22)*, 4449-4454, DOI 10.1002/adma.201503132.

[27] A. Muzaffar, M. B. Ahamed, K. Deshmukh, T. Kovářík, T. Křenek, S. K. K. Pasha, in *3D 4D Print. Polym. Nanocomposite Mater. Process. Appl. Challenges*, **2019**. 85-117, DOI 10.1016/B978-0-12-816805-9.00004-1

[28] X. Zhang, P. Yang, Y. Dai, P. Ma, X. Li, Z. Cheng, Z. Hou, X. Kang, C. Li, J. Lin, *Adv. Funct. Mater.* **2013**, *23*, 4067-4078, DOI 10.1002/adfm.201300136.

[29] H. Yang, W. R. Leow, T. Wang, J. Wang, J. Yu, K. He, D. Qi, C. Wan, X. Chen, *Adv. Mater.* **2017**, *29(33)*, 1701627, DOI 10.1002/adma.201701627.

[30] I. Roppolo, A. Chiappone, A. Angelini, S. Stassi, F. Frascella, C. F. Pirri, C. Ricciardi, E. Descrovi, *Mater. Horizons* **2017**, *4*, 396-401, DOI 10.1039/c7mh00072c.

[31] L. Ren, X. Zhou, Q. Liu, Y. Liang, Z. Song, B. Zhang, B. Li, *J. Mater. Sci.* **2018**, *53(20)*, 14274-14286, DOI 10.1007/s10853-018-2447-5.

[32] J. J. Martin, B. E. Fiore, R. M. Erb, *Nat. Commun.* **2015**, *6*, 8641,DOI 10.1038/ncomms9641.

[33] Z. Jia, Y. Yu, S. Hou, L. Wang, *J. Mech. Phys. Solids* **2019**, *125*, 178-197, DOI 10.1016/j.jmps.2018.12.015.

[34] Y. Yang, X. Li, M. Chu, H. Sun, J. Jin, K. Yu, Q. Wang, Q. Zhou, Y. Chen, *Sci. Adv.* **2019**, *5(4)*, DOI 10.1126/sciadv.aau9490.

[35] B. Wang, T. N. Sullivan, A. Pissarenko, A. Zaheri, H. D. Espinosa, M. A. Meyers, *Adv. Mater.* **2019**, *31(3)*, 1804574, DOI 10.1002/adma.201804574.

[36] L. Zorzetto, D. Ruffoni, *Adv. Funct. Mater.* **2019**, *29(1)*, 1805888, DOI 10.1002/adfm.201805888.

[37] M. Peng, Z. Wen, L. Xie, J. Cheng, Z. Jia, D. Shi, H. Zeng, B. Zhao, Z. Liang, T. Li, L. Jiang, *Adv. Mater.* **2019**, *31(35)*, 1902930, DOI 10.1002/adma.201902930.

[38] S. M. Sajadi, P. S. Owuor, S. Schara, C. F. Woellner, V. Rodrigues, R. Vajtai, J. Lou, D. S. Galvão, C. S. Tiwary, P. M. Ajayan, *Adv. Mater.* **2018**, *30(1)*, 1704820, DOI 10.1002/adma.201704820.

[39] L. Ren, B. Li, Z. Song, Q. Liu, L. Ren, X. Zhou, *Int. J. Precis. Eng. Manuf. - Green Technol.* **2019**, *6*, 89-99, DOI 10.1007/s40684-019-00030-7.

[40] J. R. Raney, B. G. Compton, J. Mueller, T. J. Ober, K. Shea, J. A. Lewis, *Proc. Natl. Acad. Sci. U. S. A.* **2018**, *115(6)*, 1198-1203, DOI 10.1073/pnas.1715157115.

[41] H. Arslan, A. Nojoomi, J. Jeon, K. Yum, *Adv. Sci.* **2019**, *6(2)*, 1800703, DOI 10.1002/advs.201800703.

[42] J. Liu, O. Erol, A. Pantula, W. Liu, Z. Jiang, K. Kobayashi, D. Chatterjee, N. Hibino, L. H. Romer, S. H. Kang, T. D. Nguyen, D. H. Gracias, *ACS Appl. Mater. Interfaces* **2019**, *11(8)*, 8492-8494, DOI 10.1021/acsami.8b17218.

[43] A. Nojoomi, H. Arslan, K. Lee, K. Yum, *Nat. Commun.* **2018**, *9*, 3705, DOI 10.1038/s41467-018-05569-8.

[44] M. Schaffner, J. A. Faber, L. Pianegonda, P. A. Rühs, F. Coulter, A. R. Studart, *Nat. Commun.* **2018**, *9*, 878, DOI 10.1038/s41467-018-03216-w.

[45] Y. Hu, A. Xu, J. Liu, L. Yang, L. Chang, M. Huang, W. Gu, G. Wu, P. Lu, W. Chen, Y. Wu, *Adv. Mater. Technol.* **2019**, *4(3)*, 1800674, DOI 10.1002/admt.201800674.

[46] S. Ma, M. Scaraggi, C. Yan, X. Wang, S. N. Gorb, D. Dini, F. Zhou, *Small* **2019**, 4(3), 1800674, DOI 10.1002/smll.201802931 [47]N. Bira, P. Dhagat, J. R. Davidson, *Front. Robot. AI* **2020**, *7*, 146.

[48] K. J. Merazzo, A. C. Lima, M. Rincó N-Iglesias, L. C. Fernandes, N. Pereira, S. Lanceros-Mendez, P. Martins, *Mater. Horiz* **2021**, *8*, 2654 DOI 10.1039/d1mh00641j.

[49] S. Malley, S. Newacheck, G. Youssef, *Addit. Manuf.* **2021**, *47*, 102239, DOI

https://doi.org/10.1016/j.addma.2021.102239

[50] F. Qiu, B. J. Nelson, *Engineering* **2015**, *1(1)*, 21-26, DOI 10.15302/J-ENG-2015005.

[51] H. Ceylan, J. Giltinan, K. Kozielski, M. Sitti, *Lab Chip* **2017**, *17*, 1705-1724, DOI 10.1039/c7lc00064b.

[52] B. Nagarajan, P. Mertiny, A. J. Qureshi, *Mater. Today Commun.* **2020**, *25*, 101520, DOI 10.1016/j.mtcomm.2020.101520.

[53] Y. Zhang, Q. Wang, S. Yi, Z. Lin, C. Wang, Z. Chen, L. Jiang, *ACS Appl. Mater. Interfaces* **2021**, *13(3)*, 4174-4184, DOI 10.1021/acsami.0c19280.

[54] S. Lucarini, M. Hossain, D. Garcia-Gonzalez, *Compos. Struct.* **2022**, *279*, 114800, DOI 10.1016/j.compstruct.2021.114800.

[55] Y. Kim, H. Yuk, R. Zhao, S. A. Chester, X. Zhao, *Nature* **2018**, *558*, 274-279, DOI 10.1038/s41586-018-0185-0.

[56] M. Gastaldi, F. Cardano, M. Zanetti, G. Viscardi, C. Barolo, S. Bordiga, S. Magdassi, A. Fin, I. Roppolo *ACS Materials Lett.* **2021**, *3*, 1, 1–17, DOI 10.1021/acsmaterialslett.0c00455

[57] M. Xie, W. Zhang, C. Fan, C. Wu, Q. Feng, J. Wu, Y. Li, R. Gao, Z. Li, Q. Wang, Y. Cheng, B. He, *Adv. Mater.* **2020**, *32*, 2000366. DOI 10.1002/adma.202000366

[58] H. Song, H. Lee, J. Lee, J. K. Choe, S. Lee, J. Y. Yi, S. Park, J.-W. Yoo, M. S. Kwon, J. Kim, *Nano Lett.* **2020**, *20*, 5185-5192, DOI 10.1021/acs.nanolett.0c01418.

[59] J. Zhang, Y. Wang, H. Pang, S. Sun, Z. Xu, L. Shen, X. Cao, C. Sun, B. Wang, X. Gong, *Compos. Part A Appl. Sci. Manuf.* **2021**, *150*, 106591, DOI 10.1016/j.compositesa.2021.106591.

[60] A. A. Kuznetsov, *J. Magn. Magn. Mater.* **2019**, *470*, 28-32, DOI 10.1016/j.jmmm.2017.10.091.

[61] W. Zhang, P. K. J. Wong, D. Zhang, J. Yue, Z. Kou, G. van der Laan, A. Scholl, J. G. Zheng, Z. Lu, Y. Zhai, *Adv. Funct. Mater.* **2017**, 27(29), 1701265, DOI 10.1002/adfm.201701265.

[62] Y. Zhang, L. Sun, Y. Fu, Z. C. Huang, X. J. Bai, Y. Zhai, J. Du, H. R. Zhai, *J. Phys. Chem. C* **2009**, *113(19)*, 8152-8157, DOI 10.1021/jp807937d.

[63] Y. I. Dikansky, D. V. Gladkikh, A. A. Zakinyan, A. G. Ispiryan, A. R. Zakinyan, *J. Mol. Liq.* **2020**, *319*, 114171, DOI 10.1016/j.molliq.2020.114171.

[64] D. Lisjak, A. Mertelj, *Prog. Mater. Sci.* **2018**, *95*, 286-328, DOI 10.1016/j.pmatsci.2018.03.003.

[65] R. M. Erb, J. J. Martin, R. Soheilian, C. Pan, J. R. Barber, *Adv. Funct. Mater.* **2016**,

26(22), 3859-3880, DOI 10.1002/adfm.201504699.

[66] L. Zhang, J. J. Abbott, L. Dong, B. E. Kratochvil, D. Bell, B. J. Nelson, *Appl. Phys. Lett.* **2009**, *94*, 064107, DOI 10.1063/1.3079655.

[67] R. M. Erb, J. S. Sander, R. Grisch, A. R. Studart, *Nat. Commun.* **2013**, *4*, 1712, DOI 10.1038/ncomms2666.

[68] S. R. Mishra, M. D. Dickey, O. D. Velev, J. B. Tracy, *Nanoscale* **2016**, *8*, 1309-1313, DOI 10.1039/c5nr07410j.

[69] A. Crivaro, R. Sheridan, M. Frecker, T. W. Simpson, P. Von Lockette, *J. Intell. Mater. Syst. Struct.* **2016**, 1-13, DOI 10.1177/1045389X15620037.

[70] J. Kim, S. E. Chung, S. E. Choi, H. Lee, J. Kim, S. Kwon, *Nat. Mater.* **2011**, *10*, 747-752,DOI 10.1038/nmat3090.

[71] H. Ceylan, I. C. Yasa, O. Yasa, A. F. Tabak, J. Giltinan, M. Sitti, *ACS Nano* **2019**, *13(3)*, 3353-3362, DOI 10.1021/acsnano.8b09233.

[72] C. Peters, O. Ergeneman, P. D. W. García, M. Müller, S. Pané, B. J. Nelson, C. Hierold, *Adv. Funct. Mater.* **2014**, *24(33)*, 5269-5276, DOI 10.1002/adfm.201400596.

[73] Y. W. Lee, H. Ceylan, I. C. Yasa, U. Kilic, M. Sitti, *ACS Appl. Mater. Interfaces* **2021**, *13(11)*, 12759-12766, DOI 10.1021/acsami.0c18221.

[74] H. C. M. Sun, P. Liao, T. Wei, L. Zhang, D. Sun, *Micromachines* **2020**, *11(4)*, 404, DOI 10.3390/MI11040404.

[75] J. Giltinan, V. Sridhar, U. Bozuyuk, D. Sheehan, M. Sitti, *Adv. Intell. Syst.* **2021**, *3(1)*, 2000204, DOI 10.1002/aisy.202000204.

[76] R. Tognato, A. R. Armiento, V. Bonfrate, R. Levato, J. Malda, M. Alini, D. Eglin, G. Giancane, T. Serra, *Adv. Funct. Mater.* **2019**, *29(9)*, 1804647, DOI 10.1002/adfm.201804647.

[77] S. Lantean, G. Barrera, C. F. Pirri, P. Tiberto, M. Sangermano, I. Roppolo, G. Rizza, *Adv. Mater. Technol.* **2019**, *29(9)*, 1804647, DOI 10.1002/admt.201900505.

[78] S. Lantean, I. Roppolo, M. Sangermano, M. Hayoun, H. Dammak, G. Rizza, *Addit. Manuf.* **2021**, *47*, 102343, DOI 10.1016/J.ADDMA.2021.102343.

[79] I. S. Novikau, P. A. Sánchez, S. S. Kantorovich, *J. Mol. Liq.* **2020**, 307, 112902, DOI 10.1016/j.molliq.2020.112902.

[80] Y. Men, W. Wang, P. Xiao, J. G Y. Men, W. Wang, P. Xiao, J. Gu, A. Sun, Y. Huang, J. Zhang, T. Chen, *RSC Adv.* **2015**, *5*, 31519-31524, DOI 10.1039/c5ra02160j.

[81] B. M. Smirnov, E. E. Son, D. V Tereshonok, *J. Exp. Theor. Phys.* **2017**, *125*, 906. DOI 10.1134/S1063776117110073.

[82] M. A. M. Gijs, *Microfluid. Nanofluidics* **2004**, *1*, 22-40, DOI 10.1007/s10404-004-0010-y.

[83] N. Pamme, *Lab Chip* **2006**, *6*, 24-38, DOI 10.1039/b513005k.

[84] N. A. Spaldin, *Magnetic Materials: Fundamentals and Applications*, **2010**. DOI 10.1017/CBO9780511781599

[85] V. S. Andreev, A. E. Luk'yanov, *Colloid J. USSR* **1990**, *51*, 643-645.

[86] Q. Wu, W. He, H.L. Liu, J. Ye, X.Q. Zhang, H.T. Yang, Z.Y Chen, Z.H Cheng *Sci. Rep.* **2013**, *3*,1547, DOI 10.1038/srep01547

[87] M. Varón, M. Beleggia, T. Kasama, R. J. Harrison, R. E. Dunin-Borkowski, V. F. Puntes, C. Frandsen, *Sci. Rep.* **2013**, *3*, 1234, DOI 10.1038/srep01234.

[88] B. D. Cullity, C. D. Graham, *Introduction to Magnetic Materials*, **2008**. DOI 10.1002/9780470386323.

[89] Z. Li, F. Yang, Y. Yin, *Adv. Funct. Mater.* **2020**, *30(2)*, 1903467, DOI 10.1002/adfm.201903467.

[90] P. Von Lockette, in *ASME 2014 Conf. Smart Mater. Adapt. Struct. Intell. Syst. SMASIS 2014*, **2014**. DOI 10.1115/SMASIS20147590

[91] H. W. Huang, M. S. Sakar, A. J. Petruska, S. Pané, B. J. Nelson, *Nat. Commun. 7*, 12263, **2016**, DOI 10.1038/ncomms12263.

[92] T. Li, J. Li, K. I. Morozov, Z. Wu, T. Xu, I. Rozen, A. M. Leshansky, L. Li, J. Wang, *Nano Lett.* **2017**, *17(8)*, 5092-5098, DOI 10.1021/acs.nanolett.7b02383.

[93] L. Bodelot, J. P. Voropaieff, T. Pössinger, *Exp. Mech.* **2018**, *58*, 207. DOI 10.1007/S11340-017-0334-7

[94] C.G. Armstrong, **1900,** US671330A.

[95] Z. Ji, C. Yan, B. Yu, X. Wang, F. Zhou, *Adv. Mater. Interfaces* **2017**, *4(22)*, 1700629, DOI 10.1002/admi.201700629.

[96] X. Cao, S. Xuan, S. Sun, Z. Xu, J. Li, X. Gong, *ACS Appl. Mater. Interfaces* **2021**, *13*, 30136. DOI 10.1021/acsami.1c08252

[97] C. H. Bennett, in *Diffus. Solids*, **1975**. DOI 10.1016/b978-0-12-522660-8.50007-6.

[98] J. R. Beeler, Jr, R. E. Dahl, Jr, R. D. Bourquin, *Le J. Phys. Colloq.* **1975**, DOI 10.1051/jphyscol:1975411.